Advances in Science and Technology Research Journal

*Advances in Science and Technology Research Journal*, 18(7), 250–263
https://doi.org/10.12913/22998624/193526
ISSN 2299-8624, License CC-BY 4.0

Received: 2024.08.07
Accepted: 2024.09.19
Published: 2024.10.06

# Investigation of Spectral Parameters of Constricted Arc Plasma for Welding Processes and Related Technologies

Valeriy Chernyak[1], Volodymyr Korzhyk[2,3], Shiyi Gao[2], Vladyslav Khaskin[2,3*], Oleksandr Voitenko[3], Yevhenii Illiashenko[3], Xinxin Wang[2,], Andrii Grynyuk[3], Oksana Konoreva[3], Iryna Sviridova [3]

[1] Taras Shevchenko National University of Kyiv, 60 Volodymyrska Str., Kyiv, 01601, Ukraine

[2] China-Ukraine Institute of Welding, Guangdong Academy of Sciences, Guangzhou, 363 Changxing Road, Tianhe, 510650, China

[3] E.O. Paton Electric Welding Institute, National Academy of Sciences of Ukraine, 11 Kazymyr Malevych Str., Kyiv, 03150, Ukraine

* Corresponding author's e-mail: vn@paton.kiev.ua

## ABSTRACT

The paper is devoted to investigation of spectral parameters of constricted arc plasma, as a foundation for further development of basic approaches to controlling of plasma-arc technologies of material treatment and welding. The relevance of application of spectrometric analysis of the welding arc consists in obtaining the possibility of sufficiently accurate control of its temperature and energy input into the product being welded, recording initiation of weld defects (internal pores), determination of atmospheric oxygen ingress into the weld pool, etc. The spectral composition, temperature and concentration of the constricted welding arc plasma were determined in the paper to more precisely define its physical characteristics at 80 and 100 A currents, in order to establish the further applicability of dynamic spectral analysis of a constricted plasma arc in control of welding processes. As modern spectrometers with CCD-detectors of the spectral range of 200 ÷ 1100 nm have the resolution of the order of 0.35 nm, which 2–3 times exceeds the quantization step by the measured wavelength, and may lead to considerable errors, an approach is proposed to increase the accuracy of spectrometric measurements to acceptable values. Radiation spectra of the constricted welding arc measured in the wavelength range of 650 ÷ 1000 nm allowed within the model of local thermodynamic equilibrium calculating the excitation temperature of the main spectral range components: Ar I and O I. It was established that the excitation temperature of electron levels of Ar atoms in the welding arc plasma only weakly depends on the discharge current, and it is equal to 13500 ± 500 K. Excitation temperature of O I electron levels was equal to 10000 ± 500 K at arc current of 100 A and to 7200 ± 500 K at 80 A current. Electron density of high-current welding arc plasma was measured by Stark broadening of Ar I lines (696.543; 772.4; 912.3 nm). It was found that with the rise of current of the constricted welding arc by 20%, an increase of charge concentration in the arc plasma by 1.5 times and of its temperature by 1.2 times are observed.

**Keywords:** spectral parameters, constricted arc plasma, spectrometric analysis, spectrometers with CCD-detectors, controlling of welding and related technologies.

## INTRODUCTION

Investigation of spectral parameters of arc plasma is of both fundamental and applied value, as it is capable of ensuring performance of contactless express-measurements [1]. Determination of plasma composition and temperature, concentration of electrons, ions, and atoms of the respective elements in the excited state, their temperatures and electric field intensity, using spectral diagnostics, allows clarifying the nature of physical phenomena at its interaction with the materials

in the welding processes [2]. Such processes include TIG [3] and GMAW [4] welding, hybrid plasma-arc welding processes [5], plasma [6] and arc surfacing [7], plasma-arc spraying [8, 9], plasma-arc cutting [10], laser-plasma cutting [11] and different methods of laser [12] and plasma [13, 14] and heat treatment of the surface. Typically, argon is used as the working gas for plasma arc and TIG processes [15]. However, to increase the efficiency of these processes, it is permissible to use an Ar+$CO_2$ mixture with a $CO_2$ content of up to 3–5% [16]. This makes it possible to use the spectral lines of argon Ar I and oxygen O I [17] in spectral studies. In addition to welding processes, spectral contactless measurements have prospects for plasma diagnostics also in other processes, for instance at waste disposal and recycling [18], metal manufacturing [19], etc.

Investigations of spectral parameters of arc plasma are relevant for intellectualization of the above-mentioned technologies, in particular they are of interest for development of systems of automated monitoring of plasma-arc welding. Such systems based on analysis of optical spectrum of welding arc radiation will allow determination of welding parameter deviation from the nominal values [20]. These deviations can be used to determine the potentially defective areas of welded joints [21]. More over, modern digital spectrometers, performing measurement of optical spectrum in several milliseconds, will enable recording the deviations of welding parameters in the real time and will allow correction of the technological parameters of the welding process to ensure the required quality of the welded joints [22, 23]. Therefore, spectral analysis can be used both for monitoring and for automation of the process of plasma-arc welding.

In addition to creation of a system of welding defect detection and automatic correction of the welding process based on spectrometer application [24], the processes of welding arc spectrometry can also provide other important additional information. Such information includes data on the influence of welded metal vapours on the welding arc [26], spectral distribution of the arc light [27], temperature parameters of the arc [28], and generation of undesirable ultraviolet (UV) radiation by the arc [29]. Such information is of interest at development of innovative intelligent welding systems [30]. Such intelligent systems should be adaptive, automated and robotic with self-teaching capability, and they should have the ability to identify the welding process, extract the necessary information from sensor signals, predict the welding process reaction to correction of welding parameters, optimize the settings and automatically eliminate the possibility of joint defect formation. In order to implement the above-listed capabilities of intelligent welding systems, a relevant approach is spectrometric analysis of welding arc parameters, providing the necessary information about it. In particular, real-time spectrometric analysis of the welding arc will allow accurately enough controlling its temperature and energy input into the item being welded, recording the initiation of weld defects (including internal defects) by the change of the intensity of spectral lines of the metals being welded, ingress of atmospheric oxygen into the weld pool, etc.

## PURPOSE, MATERIALS AND METHODS

The purpose of the work is more precise determination of the spectral composition, temperature and concentration of constricted welding arc plasma at 80 and 100 A currents to develop new approaches to application of dynamic spectral analysis of arc plasma in intelligent processes of welding and related technologies. The following tasks were solved to achieve the posed objective:

1) Development of the procedure and test facility for spectrometric studies of arc plasma with application of preliminary measurements of the contours of reference noise-free lines of plasma radiation, selection of diagnostic equipment and evaluation of its experimental capabilities.
2) Studying the spectral composition of constricted welding arc radiation in the case of transferred plasma arc at currents of 80 and 100 A.
3) Determination of excitation temperature of electron levels of atoms of the constricted welding plasma arc.
4) Determination of charge concentration in constricted welding arc plasma.
5) Elaboration of an approach to development of an control welding processes and related technologies based on feedback, which includes monitoring the spectral composition of welding arc plasma.

Investigations to solve the above tasks were performed by the following procedure:

1. Selection of materials and equipment and creation of a test facility for measurement of

experimental and simulated spectra of argon (Ar I) and oxygen (O I);
2. Measurement of profiles of noise-free radiation lines of plasma of a low-current glowing discharge in He, Ne, Kr and $H_2$, as well as radiation of He-Ne laser in a single-mode generation regime to determine the parameters of the spectrometer instrumental function;
3. Analysis of spectral composition of radiation of high-current constricted welding argon arc blown by Ar/$CO_2$ (98%Ar + 2%$CO_2$) mixture at arc currents of 80 and 100 A;
4. Determination of the temperature of the constricted welding arc plume based on calculation of excitation temperature of the main components of spectral range: Ar I and O I in the wavelength range of 650 ÷ 1100 nm at arc currents of 80 and 100 A within the model of local thermodynamic equilibrium;
5. Assessment of charge concentration in the welding arc plasma at currents of 80 A and 100 A by the width of Stark broadening of Ar I lines;
6. Analysis of the results of investigation of spectral parameters of constricted welding arc plasma and the possibilities of their application in intelligent processes of welding and related technologies.

Studied was a transferred welding plasma arc, which should run between the plasmatron tungsten electrode (cathode) and metal being welded (anode) [31]. Flat samples from AISI 304 stainless steel of 200 × 100 × 2 mm size were used as the metal being welded. Experiments were conducted in two modes of arc burning at welding current of 80 and 100 A (Table 1). Since the difference in the spectral characteristics of plasma during welding with currents of 80 and 100 A was investigated, to simplify the research, only one type of gas mixture (Ar + $CO_2$ with a $CO_2$ content of 2% [16]) with one flow rate of 30 l/min was used. The addition of $CO_2$ to the gas mixture was necessary to obtain simulated spectra of oxygen (O I).

Note that Ar I and O I spectra were studied during the conducted investigations of spectral composition of plasma of the constricted welding argon arc. Here, the questions of the influence of the metal being welded and material of plasmatron electrode on spectral characteristics of the constricted welding arc were not investigated.

## DEVELOPMENT OF A DIAGNOSTIC FACILITY AND ASSESSMENT OF ITS EXPERIMENTAL CAPABILITIES OF DIAGNOSTIC EQUIPMENT

Determination of plasma discharge parameters was performed by the measured optical emission spectra (OES) to derive the excitation temperature of electron levels of atoms and charge concentration. The schematic of optical measurements is shown in Figure 1a, and the facility assembled according to this scheme is presented in Figure 1b. Appearance of the studied constricted transferred arc is shown in Figure 1c. Argon was used as the plasma-forming gas for generation of the arc constricted by the plasma-forming nozzle of the plasmatron. From the outside, the arc was additionally constricted by a flow of shielding gas, which was a 98%Ar + 2%$CO_2$ mixture (furtheron – Ar/$CO_2$).

Measurements were performed using a spectrometer with CCD-detector S150-2-3648 USB (furtheron referred to as S150-2), which includes two diffraction spectrographs mounted in one housing with fiberoptic inputs Inp1 and Inp2. Radiation of constricted welding arc 1 passed through the wideband filter F (KC-10) for cutting off UV spectra of neighbouring orders characteristic for diffraction spectrographs. Then, part of radiation which had passed through the filer was focused by lens *L* on the inlet of optical fibre 2 of 200 μm diameter. Optical fibre divided into two equal channels Inp1 and Inp2, carried out the input of radiation to the input port of each spectrograph S150-2. Two CCD-detectors TCD1304AP (Toshiba) were used as photorecording element in S150-2. Spectral sensitivity range of these detectors is 190 ÷ 1100 nm. Taking into account the full number of pixels of the two CCD-detectors (3648 · 2 = 7296) and spectral range of 200–1100 nm, the spectrometer S150-2 provides a quantization step when recording the radiation wavelength ≈ 900/7200 = 0.125 nm at the

**Table 1.** Main technological parameters of plasma-arc welding at which the constricted arc was studied

| Welded metal | Welding current, A | Voltage, V | Welding speed, mm/min | Plasma-forming gas flow rate (Ar), l/min | Shielding gas flow rate (Ar/$CO_2$), l/min |
|---|---|---|---|---|---|
| AISI 304 steel | 80 | 23.0 | 300 | 0.8 | 30.0 |
| | 100 | 24.5 | 250 | 0.8 | 30.0 |

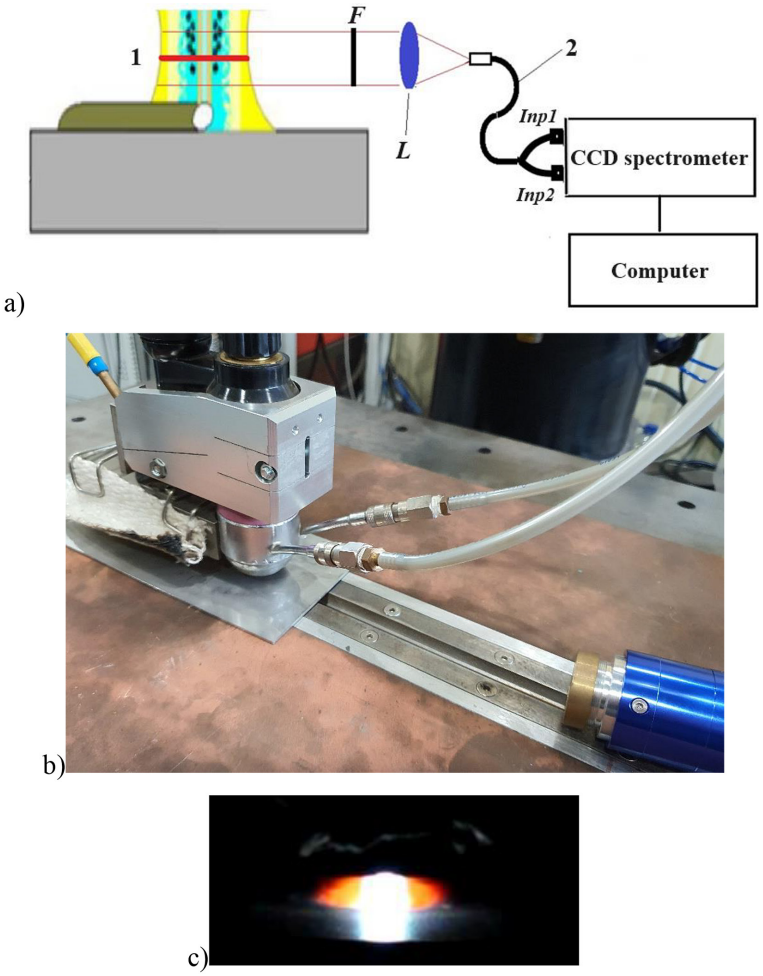


**Figure 1.** Optical spectral measurements of arc plasma: (a) – measurement scheme; (b) – equipment appearance; (c) – appearance of the studied constricted arc; 1 – constricted plasma arc; 2 – optical fibre; F – filter, L – lens; Inp1, Inp2 – fiber optic inputs into the spectrometer

resolution of spectrometer S150-2 of ≈ 0.35 nm according to certificate data.

The commensurability of the spectrometer resolution with the quantization step by wavelength λ actually leads to an extremely small number of values in the instrumental function, resulting in large errors both at determination of maximal values of the function and its area. Therefore, considering the features of the known methods [32] of radiation spectra processing to determine the parameters of the instrumental function of the spectrometer, the contours of noise-free lines of plasma radiation in low-current (~5 mA) glowing discharge in $H_2$ ($H_\alpha$, $H_\beta$), He (667.82; 501.57 nm), Ne (703.24 nm), Kr (427.4; 437.228 nm) and radiation of He-Ne laser in single-mode generation regime (632.8 nm) were measured. Such evaluation of the instrumental function indicated a Gaussian contour with spectral line full width at half maximum (FWHM) of 0.3 nm (Fig. 2). At assessment of the spectrometer instrumental function, the maximal intensity of plasma radiation lines $I_0$ was determined in arbitrary units (au). The graphs given in Figure 2 allowed evaluation of broadening of the measured spectral lines to be taken into account in further research. So, the accuracy of temperature determination becomes lower, as broadening of the spectral lines used for calculations decreases.

## RESEARCH RESULTS

### Investigation of spectral composition of constricted welding plasma arc radiation

As follows from comparison of Ar I and O I experimental spectra with the respective simulated Ar I and O I spectra, the main components of plasma emission spectrum in the range of

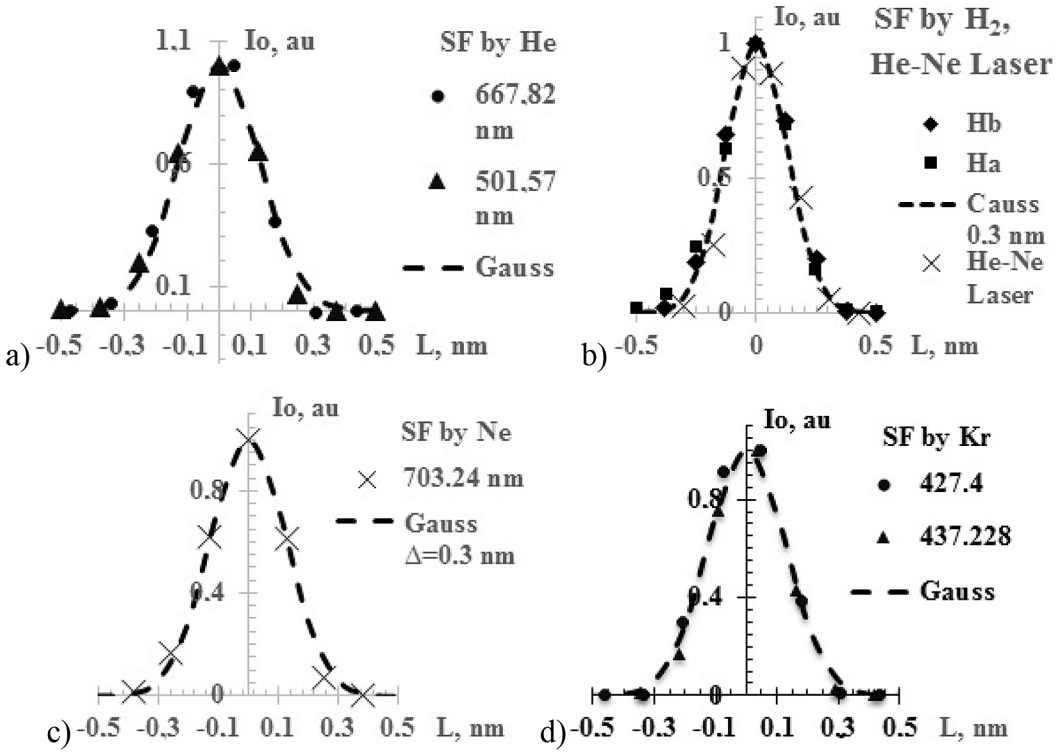


**Figure 2.** Measured profiles of noise-free lines of plasma radiation of low-current (~ 5 mA) glowing discharge in: (a) He (667.82; 501.57 nm); (b) $H_2$ ($H_\alpha$, $H_\beta$) and radiation of He-Ne laser in single-mode generation regime (632.8 nm); (c) Ne (703.24 nm); (d) Kr (427.4; 437.228 nm). Experimental data are denoted by markers; simulated Gaussian profile of width Δ = 0.3 nm at half maximum is shown by a dashed line

wavelengths of 650 ÷ 1000 nm of a high-current welding argon arc, blown by a shielding gas mixture of Ar/$CO_2$ (98/2), were the lines shown in Figure3. Spectra simulation was performed taking into account all the lines of NIST base [33] for Ar I and O I for equilibrium plasma, and the instrument profile of spectrometer S150-2 used in the experiment (Gaussian profile of width $\Delta\lambda_{1/2}^{in}$ 0.3 nm at half-maximum of intensity FWHM) at excitation temperatures $T^{*e}$ of Ar I and O I electron levels, determined during the experimental investigations.

In the case of a constricted arc current of 100 A (Fig. 3a), practically all the lines of experimental spectra, coinciding by intensity with the simulated ones, were used for investigations. In the case of 80 A current (Fig. 3b), such a coincidence was only characteristic for three wavelengths,

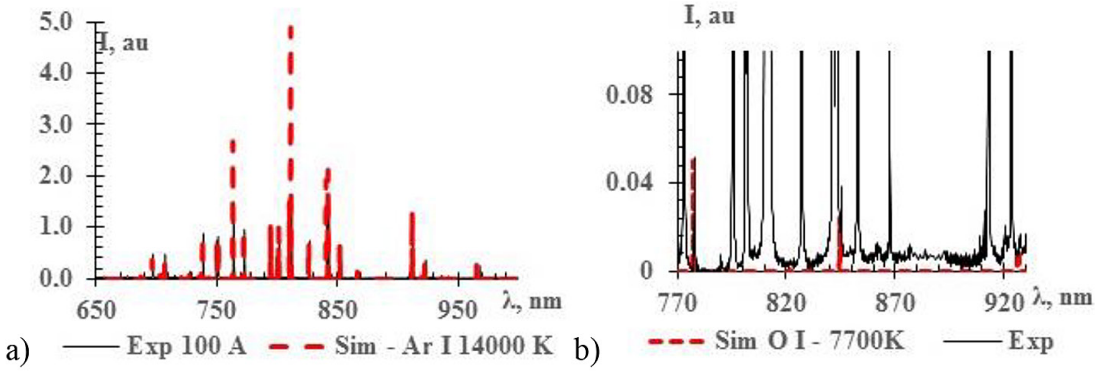


**Figure 3.** Plasma spectra in wavelength range of 650 ÷ 1000 nm of a high-current welding arc blown by a Ar/$CO_2$ (98/2) mixture at the following arc currents: (a) 100 A, (b) 80 A. The solid black lines are the experimental spectra. Simulated Ar I spectra at $T^{*e}$ = 14000 K (a) and O I spectra at $T^{*e}$ = 7700 K (b) are designated by a dashed red line. All the spectra are normalized to the intensity of a weak Ar I line at λ = 801.5 nm

from which two were selected for further investigations (696.543 and 706.72 nm). Selection of lines for analysis is due to the need to eliminate the phenomenon of radiation self-absorption. It is known that self-absorption is the smaller, the lower the line intensity. Therefore, lines of experimental spectrum, with the intensity approximately 5 times smaller than the maximal intensity of simulated spectrum lines, were selected for further analysis.

#### Determination of excitation temperature of a constricted welding arc

Based on the spectra, observed in wavelength range of 650 ÷ 1000 nm, we calculated within the model of local thermodynamic equilibrium (LTE) the excitation temperature of the main components of this spectral range: Ar I and O I. In LTE model it is assumed that electron distribution on energy levels is completely determined by particle collisions, and the collision processes occur so often that at any change of the conditions in the plasma the respective distribution is established instantly. Population of excited electron levels of atoms in LTR-plasmas is determined by Boltzmann formula (3):

$$N_n = N_0 \frac{g_n}{g_0} exp\left(-\frac{E_n}{k\,T}\right) \quad (1)$$

where: $N_n$ is the concentration of excited atoms in state $n$, $N_0$ is the atom concentration in the ground state, $g_n$ and $g_0$ are the statistical weights of the excited and ground states, respectively. Intensity $I_{nk}$ of spectral line for equilibrium plasma is:

$$I_{nk} \sim A \frac{g_k f_{kn}}{g_n \lambda^3} N_n \quad (2)$$

Spectral line intensity $I_{nk}$ was determined as power, emitted by a unit of object volume in the wavelength range, corresponding to full width of this spectral line:

$$I = \int_{\lambda_1}^{\lambda_2} I_\lambda \, d\lambda \quad (3)$$

where: $I_\lambda$ is the spectral radiation power, corresponding to this wavelength $\lambda$. Integration was carried out along the Voigt contour with width at half maximum (FWHM) of the respective Ar I lines of experimental spectra $\Delta_{exp}$, which, as known from work [33], is the convolution of the Gaussian and Lorentzian contours forming it:

$$I(x) = \int_{-\infty}^{\infty} G(x')L(x-x')dx' \quad (4)$$

Here, particular attention was paid to the satisfactory agreement between the experimental profiles of the used lines and simulations of the Voigt contour (Fig. 4). Integration limits were selected up to such wavelengths, where $I_\lambda$ practically drops to zero, taking into account the known recommendations of work [35] on selection of integration limits of extended contours.

A fundamental difference of the recorded spectrum components, corresponding to highlighting of oxygen atoms, from argon atoms, was their multiplicity with unresolved multiplet profiles in good agreement with the profiles in the simulated O I spectra, taking into account only the instrumental profile with ΔG = 0.3 nm for each multiplet component (Fig. 5).

Taking into account the unresolved structure of O I multiplets 777 (7771.94; 7774.17; 7775.39 nm), 844 (8446.25; 8446.36; 8446.76 nm), 926 (9260.81; 9260.85; 9260.94; 9262.58; 9262.67;

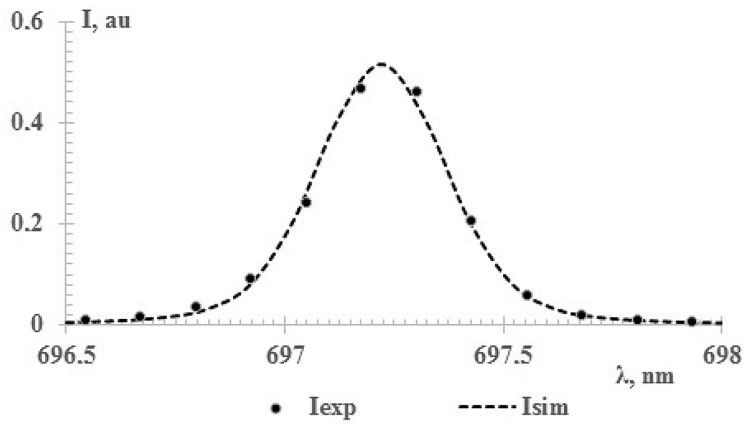


**Figure 4.** Superposition of simulated Voigt contour on the contour of Ar I line with λ = 696.543 nm of arc plasma spectrum at 100 A discharge current

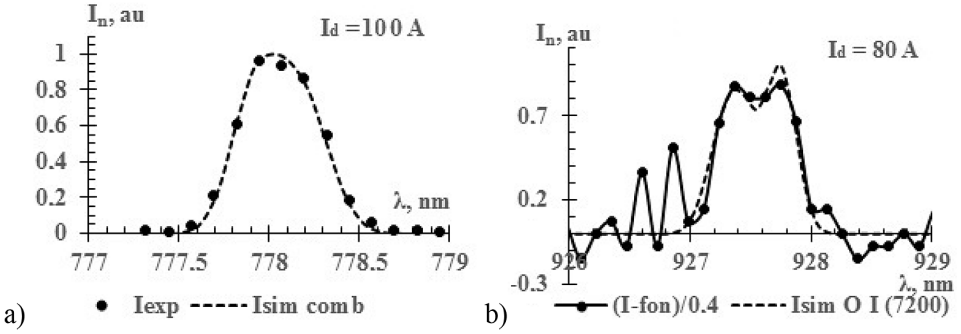


**Figure 5.** Profiles of unresolved O I multiplets (777 nm) (a) and O I multiplet (926 nm) (b) in the arc spectrum $I_{exp}$ (●) at plasma arc currents of 100 A (a) and 80 A (b) and of those simulated with Gaussian profile ΔG = 0.3 nm of each line in $I_{exp}$ multiplets for $T_0^{*e}$ = 10000 K (a) and $T_0^{*e}$ = 7200 K (b).

9262.78; 9265.83; 9265.93; 9266.01 nm) and good agreement of their experimental profiles $I_{exp}$ with the respective profiles in simulated spectra $I_{sim}$, in order to determine the excitation temperature of O I electron levels – $T_0^{*e}$ – we used calibration dependences of the ratios of the intensity maxima of two multiplets $I_{844}/I_{777}$ and $I_{926}/I_{777}$ on the excitation temperature in the simulated O I spectra in the range of change $T_0^{*e}$ = 1000 ÷ 20000 K (Fig. 6). Calibration curves are given in Figure 6 and they are in satisfactory agreement with Equations 5–6.

$$y = 239202x^6 + 24427x^5 - 160106x^4 + 117076x^3 - 26266x^2 + 9899.4x + 640.09 \quad (5)$$

$$y = 239202x^6 + 24427x^5 - 160106x^4 + 117076x^3 - 26266x^2 + 9899.4x + 640.09 \quad (6)$$

where: $y$ is the excitation temperature of electron levels of oxygen atom $T_0^{*e}$, and x are the ratios of intensities of two multiplets $I_{926}/I_{777}$ (5) и $I_{844}/I_{777}$ (6).

Derived values of excitation temperature of O I electron levels were equal to 10000 ± 500 K at constricted arc discharge current of 100 A and to 7200 ± 500 K at discharge current of 80 A. Boltzmann diagrams to determine the excitation temperature of Ar I electron levels were plotted using the following line intensities: 6752.83; 6871.29; 6938; 6965.43; 7067.22; 9657.78 and 9784.5 nm (Fig. 7).

As follows from the data given in Fig. 7, the excitation temperature of electron levels of Ar atoms in the welding arc plasma weakly depends on discharge current and is equal to 13500 ± 500 K.

Significantly smaller values of excitation temperature of electron levels of O atoms, compared to Ar atoms in radiation spectra integrated along the line-of-sight, as well as the above noted differences of their line profiles in emission spectra of high-current welding arc plasma in a flow of $Ar/CO_2$ gas mixture, point to fundamental differences in radial distributions of Ar and O atom concentrations (predominantly presence of oxygen atoms in the plasma plume peripheral zone).

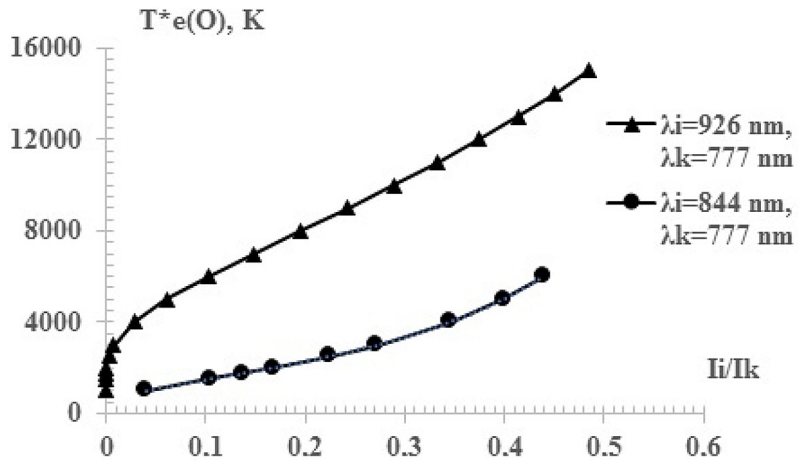


**Figure 6.** Calibration dependencies $T_0^{*e}$ ($I_{844}/I_{777}$) – 1 and $T_0^{*e}$ ($I_{926}/I_{777}$) – 2

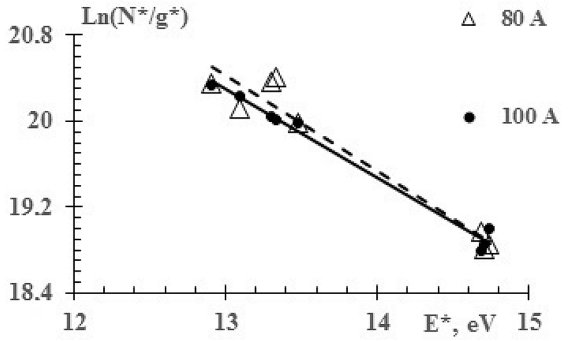


**Figure 7.** Boltzmann diagrams of Ar I for welding arc plasma at discharge currents of 80 and 100 A

## Determination of concentration of constricted welding arc plasma

Electron density of high-current welding arc plasma was measured using Stark broadening of Ar I lines (696.543; 772.4; 912.3 nm). As was noted above, experimental profiles of Ar I lines were well approximated by the peak profile of Voigt function, which in its turn is a convolution of the Gaussian and Lorentzian profiles. Most often, the expansion mechanisms, taken separately, create either a Gaussian or Lorentzian profile. If the Gaussian or Lorentzian components are comparable, the final form of *V(x)* will be the Voigt function [36]. The Voigt function can be calculated by the following formula [37]:

$$V(x,a) = \frac{a}{\pi} \times \int_{-\infty}^{\infty} \frac{e^{-t^2}}{a^2+(x-t)^2} \times \, dt \qquad (7)$$

$$x = \frac{\lambda-\lambda_{ul}}{\Delta\lambda_{1/2}^{G}} \times 2 \times (ln2)^{1/2} \qquad (8)$$

$$a = \frac{\Delta\lambda_{1/2}^{L}}{\Delta\lambda_{1/2}^{G}} \times (ln2)^{1/2} \qquad (9)$$

As is known, convolution of two Gaussian profiles leads to also a Gaussian profile with half-width $\Delta_G$, equal to the square root of the sum of squares of the half-widths of the original profiles. At convolution of two Lorentzian profiles we again obtain a Lorentzian profile, the half-width of which is equal to the sum of half-widths of the initial contours [38]. Owing to Doppler effect, the line profile is readily described by Gaussian profile with the width at half-maximum [39]

$$\Delta\lambda_{1/2}^{D} = \lambda_0 \left(8ln2 \frac{k_B T_g}{m_a c^2}\right)^{1/2} \qquad (10)$$

where: $k_B$ is the Boltzmann constant (unit of measurement: $J \cdot K^{-1}$), $T_g$ is the gas temperature in K, $m_a$ is the emitter weight in kg, c is the speed of light in $m.s^{-1}$. For Ar plasma with gas temperature $T_g$ = 13500 K $\Delta\lambda_{1/2}^{D} \approx 1.32 \cdot 10^{-5} \cdot \lambda_0$, which for optical range lines is significantly smaller than the width at half-maximum of the instrumental function ( $\Delta\lambda_{1/2}^{in}$ = 0.3 nm).

To assess the width of the Lorentzian component $\Delta\lambda_{1/2}^{L}$ in the measured profiles of Ar I lines, we used the graphic presentation of $\Delta\lambda_{1/2}^{L}\Delta\lambda_{1/2}^{F}$= f($\Delta\lambda_{1/2}^{G}/\Delta\lambda_{1/2}^{F}$) dependence [34, 36] (Fig. 8), which was approximated by the following polynomial:

$$\Delta\lambda_{1/2}^{L}/\Delta\lambda_{1/2}^{F} = -0.9212/\Delta\lambda_{1/2}^{F})^2 - \\ - 0.0813/\Delta\lambda_{1/2}^{F}) + 1.0015 \qquad (11)$$

For our case in equation (12) $\Delta\lambda_{1/2}^{G} = \Delta\lambda_{1/2}^{in}$ = 0.3 nm and $\Delta\lambda_{1/2}^{F}$ is the contour width at half-maximum of intensity of selected Ar I line in the measured spectrum. The thus obtained $\Delta\lambda_{1/2}^{L}$ and $\Delta\lambda_{1/2}^{G}$ values for a series of Ar I lines are given in Table 2.

As is known [34], Lorentzian profiles of lines, emitted by atoms or ions, which are in a dense gas or plasma, are chiefly determined by interaction of the radiators with the surrounding particles. This type of line broadening is usually called pressure broadening. In physical terms, pressure broadening is subdivided into: resonance, Van der Waals and Stark, depending on whether the expansion is due to interaction:

a) with atoms of the same kind (atoms in one of the states, transition between which leads to emission of this line, interact with atoms in the ground state);
b) with atoms or molecules of another kind or atoms of the same kind, but not in the ground state;
c) with charged particles, i.e. ions and electrons.

Note that resonance broadening of the lines is practically absent in lines, for which the transition from the lower state into the ground state is prohibited by selection rules [37, 39]. Stark broadening is of special interest for plasma diagnostics. Knowledge of its profile allows quite accurate determination of charge concentration in the plasma [40, 41].

Therefore, for weaker lines, where profile distortion is practically absent due to self-absorption, and where transition from the lower to the ground state is prohibited by selection rules, we

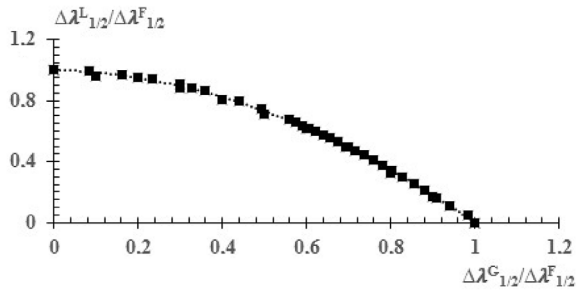


**Figure 8.** Connection of the width of Voigt profile $\Delta_F$ with the widths of its Gaussian $\Delta_G$ and Lorentzain components $\Delta_L$

could calculate an estimate of Stark profile width $\Delta_S$ using the following equation:

$$\Delta\lambda^S_{1/2}\Delta s = \Delta\lambda^L_{1/2} - \Delta\lambda^{VdW}_{1/2} \quad (12)$$

where: $\Delta\lambda^{VdW}_{1/2}$ is the width at half-maximum of Van den Waals profile.

$\Delta\lambda^{VdW}_{1/2}$ calculation was conducted using the following equations, in keeping with Lindholm-Foley theory [37, 42, 43]:

$$\Delta\lambda^{VdW}_{1/2} = \frac{\lambda^2_{ul}}{2\times\pi\times c} \times 8.16 \times (C_6)^{2/5} \times \bar{v}^{3/5} \times N_g \quad (13)$$

where: $\bar{v}$ is the mean velocity between the radiators and perturbers,

$$\bar{v} = \left(\frac{8 \times k_B \times T_g}{\pi \times \mu}\right)^{1/2} \quad (14)$$

Reduced mass $1/\mu = 1/m_a + 1/m_b$ with $m_a$ and $m_b$ – masses of radiators and perturbers, respectively. $C_6$ is the Van der Waals constant, which is included into Van der Waals potential $\Delta V_{VdW} \approx - C_6/r^6$, $r$ is the separation distance.

$$C_6 = \frac{1}{\hbar} \times e^2 \times \alpha \times a_0^2 \times (\overline{R_u^2} - \overline{R_l^2}) \quad (15)$$

where: $h$ is the Plank constant, α and $a_0$ are the mean polarizability of exciting particles (for Ar α = 1.64 × $10^{-24}$ $cm^{-3}$) and Bohr radius ($a_0$ = 5.29 × $10^{-9}$cm. $\overline{R_u^2}$ and $\overline{R_l^2}$ are the root-mean-square radii of levels u and l), respectively. In Coulombian approximation of $\overline{R_u^2}$ and $\overline{R_l^2}$ values:

$$\overline{R_j^2} = \frac{n_j^{*2}}{2} \times \left[5 \times n_j^{*2} + 1 - 3 \times l_j \times (l_j + 1)\right] \quad (16)$$

where: $l_j$ is the orbital quantum number and $n_j^{*2}$ is the square of effective quantum number of level $j$, respectively.

$$n_j^{*2} = \frac{E_{Ryd}}{E_{ion} - E_j} \quad (17)$$

where: $E_{Ryd}$ denotes Rydberg constant $E_{Ryd}$ = 109 737.3 $cm^{-1}$, $E_{ion}$ is the radiator ionization energy (for Ar $E_{ion}$ = 127109.7 $cm^{-1}$), and $E_j$ is the excitation energy of level j.

Results of $\Delta_{vdW}$ calculation, using equations (13–17) for lines with lower metastable state, are given in Table 3 at 100 A arc current.

Proceeding from the ratio of calculated values of Van der Waals broadening and experimental broadening values (Table 2) and the known weak nonmonotnic dependence of this broadening on gas temperature [44–46] for argon lines, ending at metastable levels, we were able to neglect $\Delta\lambda^{VdWL}_{1/2}$ contribution into $\Delta\lambda^L_{1/2}$ and to assume that $\Delta\lambda^L_{1/2} \approx \Delta\lambda^S_{1/2}$. Determination of plasma electron concentration $N_e$ by the values of full widths at half-maximum (FWHM) derived by the above-described methods for Stark profiles $\Delta\lambda^S_{1/2}$ $\Delta\lambda^S_{1/2}$ was conducted using formula [36, 47]:

$$\Delta_s \approx 2\left[1 + 1.75 \cdot 10^{-4} N_e^{1/4} \alpha \left(1 - 0.068 N_e^{1/6} T^{-1/2}\right)\right] \times 10^{-16} \omega N_e \quad (18)$$

where: $[\Delta s] = Å$; $[N_e]$ = $cm^{-3}$; $[T]$ = K; $\alpha$, $\omega$ are the tabulated Grim parameters [22, 29].

**Table 3.** Results of calculation of the components of Van de Waals and Lorentzian profiles at half-maximum at 100 A arc current

| λ, nm | $\Delta\lambda^{VdWL}_{1/2}$ nm | $\Delta\lambda^L_{1/2}$ nm |
|---|---|---|
| 696.543 | 1.84E-03 | 0.119 |
| 772.4 | 2.26E-03 | 0.149 |
| 912.3 | 3.16E-03 | 0.103 |

**Table 2.** Width of the components of Voigt, Gauss and Lorentzian profiles at half-maximum for 80 and 100 A currents of the plasma arc

| Parameter | 80 A | | | 100 A | | |
|---|---|---|---|---|---|---|
| λ, nm | $\Delta\lambda^F_{1/2}$, nm | $\Delta\lambda^G_{1/2}$, nm | $\Delta\lambda^L_{1/2}$, nm | $\Delta\lambda^F_{1/2}$, nm | $\Delta\lambda^G_{1/2}$, nm | $\Delta\lambda^L_{1/2}$, nm |
| 696.543 | 0.34 | 0.30 | 0.07 | 0.37 | 0.30 | 0.12 |
| 772.4 | 0.35 | 0.30 | 0.09 | 0.39 | 0.30 | 0.15 |
| 912.3 | 0.35 | 0.30 | 0.09 | 0.36 | 0.30 | 0.10 |

According to work [36], formula (18) is sufficiently accurate as long as the following inequalities are satisfied

$$10^{-14}\alpha N_e^{1/4} < 0.5 \quad (19)$$

$$\sigma = 8.0 \cdot 10^{-2}\omega\lambda^{-2}(\frac{T}{\mu})^{-1/2}N_e^{2/3} > 1 \quad (20)$$

$$R = 9.0 \cdot 10^{-2}N_e^{\frac{1}{6}}T_e^{-\frac{1}{2}} < 0.8 \quad (21)$$

where: $\mu$ is the radiator atomic weight, [λ] = Å, while $\sigma$ and R are the criteria accepted in work [36].

According to work [47], experiments confirmed the high accuracy of formula (18), and the limit charge concentration, relating the concentration to Stark broadening parameter:

$$N_{el} \approx 10^{18}\lambda^{7/2}\omega^{-7/4}\text{cm}^{-3} \quad (22)$$

where: $\lambda$ is the wave length in μm.

Results of evaluation of charge concentration in the welding arc plasma at 80 A and 100 A currents by the width of Stark broadening of Ar I lines ending in metastable states (696.543; 772.4 and 912.3 nm) are given in Table 4. According to the data of Table 4, mean value of concentration $N_e$ of charges in the plasma of a constricted welding arc at 80 A current was equal to (5.7 ± 0.8) · $10^{16}$ $cm^{-3}$, and at 100 A current it was (8.6 ± 0.7) · $10^{16}$ $cm^{-3}$. Thus, at 20% increase of arc current the charge concentration in it increases 1.5 times, leading to 1.2 times rise of arc temperature.

## DISCUSSION

During the research, welded joints of AISI 304 steel samples with a thickness of 2 mm were obtained (Fig. 9). The quality of the welds was satisfactory. During the welding process, the spectra of argon (Ar I) and oxygen (O I) were studied using optical emission spectroscopy to determine the spectral composition, temperature and concentration of the welding plasma of the compressed arc at currents of 80 and 100 A. The issue of quality control of weld formation using spectroscopy was not considered at this stage of the research.

Parameters of plasma of a constricted welding argon arc shielded by an enveloping flow of Ar/$CO_2$ gas mixture, such as excitation temperature and density of electron have been studied using optical emission spectroscopy of plasma parameters. It was found that the main components of plasma radiation spectrum for optical range of 650 ÷ 1000 nm are the lines of argon and oxygen atoms, while metal lines are practically absent. Ar I and O I line profiles differed significantly both by their width at half-maximum, and by their shape: profile of Ar I lines is Voigt, and that of O I lines is Gaussian. Width of Ar I line contours at half-maximum (FWHM) noticeably exceeded the width of instrumental (Gaussian) function of the spectrometer, and FWHM for O I lines corresponded to the instrumental function.

Excitation temperature of Ar I levels $T_{Ar}^{*e}$ was considerably higher than $T_O^{*e}$ temperature. $T^*$ dependencies on arc current also turned out to be different: change of arc current by 20% practically did not influence $T^*$(Ar I) value, but it led to a directly proportional change of $T^*$(O I) by 30%. Such features of $T^*$(I) of argon and oxygen atoms, as well as the above-mentioned differences in their line profiles in emission spectra of plasma of high-current welding argon arc in a shielding flow of Ar/$CO_2$ gas mixture, point to fundamental differences in radial distributions of Ar and O atom concentration (predominance of oxygen atoms in the peripheral zone of the plasma plume).

Note the fact that a change in arc current by 20% was accompanied by practical absence of

**Table 4.** Concentration $N_e$ of charges in the plasma of a constricted welding arc at 80 A and 100 A currents by the width of Stark broadening of Ar I lines

| λ, nm | $N_e$, $cm^{-3}$ | $N_{el}$, $cm^{-3}$(22) | $10^{-14}\alpha N_e^{1/4}$ (19) | σ (20) | *R* (21) |
|---|---|---|---|---|---|
| 80 A | | | | | |
| 696.543 | $5.5 \cdot 10^{16}$ | $3.8 \cdot 10^{19}$ | $4.4 \cdot 10^{-12}$ | 0.8 | 0.5 |
| 772.4 | $5.0 \cdot 10^{16}$ | $3.2 \cdot 10^{19}$ | $3.5 \cdot 10^{-12}$ | 0.8 | 0.5 |
| 912.3 | $6.6 \cdot 10^{16}$ | $9.7 \cdot 10^{19}$ | $4.6 \cdot 10^{-12}$ | 0.5 | 0.5 |
| 100 A | | | | | |
| 696.543 | $9.0 \cdot 10^{16}$ | $3.8 \cdot 10^{19}$ | $5.0 \cdot 10^{-12}$ | 1.1 | 0.5 |
| 772.4 | $9.0 \cdot 10^{16}$ | $3.2 \cdot 10^{19}$ | $4.1 \cdot 10^{-12}$ | 1.2 | 0.5 |
| 912.3 | $7.8 \cdot 10^{16}$ | $9.7 \cdot 10^{19}$ | $4.8 \cdot 10^{-12}$ | 0.6 | 0.5 |

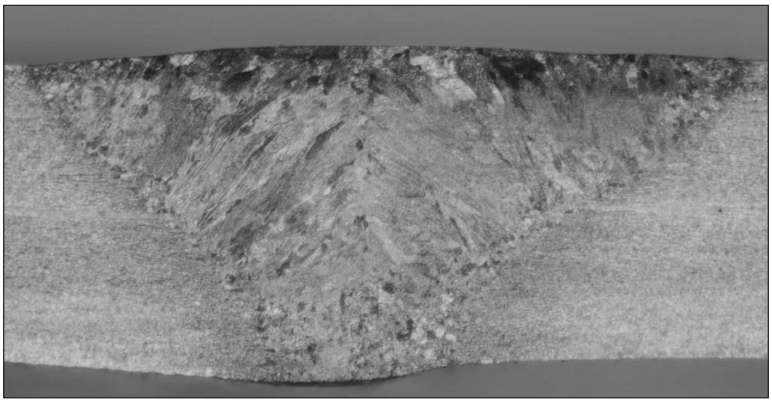

**Figure 9.** The structure of the weld obtained on AISI 304 steel 2 mm thick using plasma welding (Table 1)

*T**(Ar I) change and a marked change in charge concentration. The latter can be related to a significant influence of metal vapours on the degree of plasma ionization.

Owing to a broad spectral range of CCD-detector sensitivity (190 ÷ 1100 nm), and their sufficiently fast response (from 4 ms), it becomes possible to analyze the spectral composition of welding arc plasma by pre-selected lines [47]. Such an analysis can be dynamic, i.e. performed directly during welding. It can be built-in into the welding control system through the above-mentioned respective feedbacks. We can also limit ourselves to recording the deviations from process stability to determine the zones of post weld control of the weld. Spectral analysis of the welding arc can allow recording the following aspects: change of total temperature (energy) of plasma by the change of the parameter of excitation temperature *T** of O I electron levels; influence of the welded metal vapours on the degree of plasma ionization

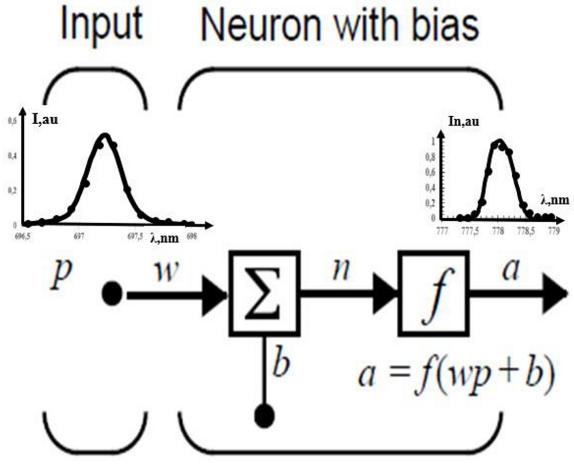


**Figure 10.** Schematic of neural network operation

and, respectively, on welding process stability by the change of charge concentration parameter $N_e$. It will enable implementing the system of monitoring and control of the welding processes, based on spectral analysis of the welding arc.

In further use of spectral analysis of the welding arc, it is advisable to use a self-learning neural network as the basis of control and feedback system for welding processes. Such a neural network can be used to continuously compare the initially measured reference spectral composition of the welding arc (*p*) with the arc spectral composition at the given moment of time (*a*) during welding or surfacing (Fig. 10). It will enable determination of displacement value (*b*) and monitoring it during the welding (surfacing) process [42]. If value *b* is within the admissible limits, the welding process can be considered to provide the result of the required quality. If value *b* exceeds the admissible limits, the feedback is used to eliminate the respective value of process disturbance.

Such neural networks will allow performance of self-teaching of welding equipment, and in the future replacing the welding operator as much as possible. Here, the information about the welding arc spectral composition, its luminosity and visually recorded behaviour can be analyzed by the neural networks and can improve the welding process control. Thus, information on the spectral composition of the welding arc will form the basis of feedback system operation.

## CONCLUSIONS

Conducted in the range of 650 ÷ 1000 nm wavelengths comparison of experimental spectra of Ar I argon atom and O I oxygen atom with the

respective simulated spectra of high-current welding argon arc blown by a shielding $Ar/CO_2$ gas mixture (98/2) showed that Ar I lines and O I multiplets are the main components of the plasma emission spectrum. Measured in 650 ÷ 1000 nm wavelengths radiation spectra of welding plasma arc allowed within the model of local thermodynamic equilibrium calculating the excitation temperature of the main components of Ar I and O I spectral range. It was established that the excitation temperature of Ar atom electron levels in welding arc plasma only weakly depends on the discharge current, and it is equal to 13500 ± 500 K. The excitation temperature of O I electron levels was equal to 10000 ± 500 K at arc current of 100 A and to 7200 ± 500 K at current of 80 A. Significantly lower values of excitation temperature of O atom electron levels, compared to Ar atoms in line-of-sight integrated spectra point to a predominant presence of oxygen atoms in the peripheral zone of the plasma plume. Electron density of plasma in the high-current welding arc was measured using Stark broadening of Ar I lines (696.543; 772.4; 912.3 nm). It was established that with increase of current of the compressed welding arc by 20% an increase of charge concentration in the arc plasma by 1.5 times and of its temperature by 1.2 times is observed.

## Acknowledgments

The work was funded within the following programs:

- Strategic project of the Academy of Sciences of Guangdong Province, (GDAS'Project of Science and Technology Development, 2020GDASYL-20200301001), China.
- The National Key Research and Development Program of China – in the framework of the strategy "One Belt – One Road" (grant number 2020YFE0205300), China.
- The National Key Research and Development Program of China (Project Number: 2023YFE0201500).

## REFERENCES

1. Mirapeix J., Cobo A., Fuentes J., Davila M., Etayo J.M., Lopez-Higuera J.-M. Use of the plasma spectrum RMS signal for arc-welding diagnostics. Sensors, 2009, 9, 5263–5276. [https://doi.org/10.3390/s90705263]
2. Gu, Y., Xu, Y., Shi, Y., Feng, C., Volodymyr, K. Corrosion resistance of 316 stainless steel in a simulated pressurized water reactor improved by laser cladding with chromium. Surface and Coatings Technology, 2022, 441, 128534 (https://doi.org/10.1016/j.surfcoat.2022.128534)
3. Prilutskyi V.P., Petrichenko I.K. Influence of oxygen concentration in argon of the protective nozzle on the properties and colour of weld surface in TIG welding of titanium // The Paton Welding Journal, 2021, 7, 7–12. [https://doi.org/10.37434/tpwj2021.07.02]
4. Zhanga W., Xua Y., Shia Y., Sua G., Gua Y., Volodymyr K. Intergranular corrosion characteristics of high-efficiency wire laser additive manufactured Inconel 625 alloys. Corrosion Science, 2022, 205, 110422. [https://doi.org/10.1016/j.corsci.2022.110422]
5. Gu Y., Xu Y., Shi Y., Feng C., Volodymyr K. Corrosion resistance of 316 stainless steel in a simulated pressurized water reactor improved by laser cladding with chromium. Surface and Coatings Technology, 2022, 441, 128534. [https://doi.org/10.1016/j.surfcoat.2022.128534]
6. Korzhyk V., Khaskin V., Grynyuk A., Ganushchak O., Peleshenko S., Konoreva O., Demianov O., Shcheretskiy V., Fialko N. Comparing features in metallurgical interaction when applying different techniques of arc and plasma surfacing of steel wire on titanium. Eastern-European Journal of Enterprise Technologies, 2021, 4, 12(112), 6–17. [https://doi.org/10.15587/1729-4061.2021.238634]
7. Babinets A.A., Ryabtsev I.O., Lentyugov I.P., Ryabtsev I.I., Kaida T.V., Bogaichuk I.L. Influence of amplitude and frequency of oscillations of electrode wire in arc surfacing on formation and structure of the deposited metal and penetration of base metal. The Paton Welding Journal, 2020, 10, 23–30. [https://doi.org/10.37434/tpwj2020.10.05]
8. Grigorenko G.M., Adeeva L.I., Tunik A.Y., Korzhik V.N., Doroshenko L.K., Titkov Y.P., Chaika A.A Structurization of coatings in the plasma arc spraying process using B4C + (Cr, Fe)7C3-cored wires. Powder Metallurgy and Metal Ceramics, 2019, 58(5–6), 312–322. [http://dx.doi.org/10.1007/s11106-019-00080-1]
9. Chen Y., Liang X., Wei S., Chen X., Xu B. Numerical simulation of the twin-wire arc spraying process: Modeling the high velocity gas flow field distribution and droplets transport. J. Therm. Spray Tech., 2012, 21, 263–274. [https://doi.org/10.1007/s11666-011-9723-0]
10. Deli J., Bo Y. An intelligent control strategy for plasma arc cutting technology. Journal of Manufacturing Processes, 2011, 13(1), 1–7. [https://doi.org/10.1016/j.jmapro.2010.08.003]
11. Fialko, N.M., Prokopov, V.G., Meranova, N.O.,

Korzhik, V.N., Sherenkovskaya, G.P. Thermal physics of gasothermal coatings formation processes. State of investigations. Fizika i Khimiya Obrabotki Materialov, 1993, (4), 83–93.

12. Vora H.D., Dahotre N.B. Laser surface heat treatment and modification. AM&P Technical Articles, 2013, 171(11): 45–47. [https://doi.org/10.31399/asm.amp.2013-11.p045]
13. Hryhorenko G.M., Adeeva L.I., Tunik A.Y., Karpets M.V., Korzhyk V.N., Kindrachuk M.V., Tisov O.V. Formation of microstructure of plasma-arc coatings obtained using powder wires with steel skin and B4C + (Cr, Fe)7C3 + Al filler. Metallofizika i Noveishie Tekhnologii, 2020, 42(9), 1265–1282. [https://doi.org/10.15407/mfint.42.09.1265]
14. Chabak Yu.G., Pastukhova T.V., Efremenko V.G., Zurnadzhy V.I., Fedun V.I., Tsvetkova E.V., Dzherenova A.V. Pulsed plasma surface modification of grey cast iron. Journal of Physical Studies, 2020, 24(2), 2501 [8 pages]. [https://doi.org/10.30970/jps.24.2501]
15. Klett J., Bongartz B., Wolf T., Hao C., Maier H. J., Hassel T. Plasma welding of aluminum in an oxygen-free argon atmosphere. Advances in Materials Science, 2023, 23, 1(75), 5–18. [https://doi.org/10.2478/adms-2023-0001]
16. Shanping L., Hidetoshi F., Kiyoshi N. Effects of $CO_2$ shielding gas additions and welding speed on GTA weld shape. Journal of Materials Science, 2005, 40(9): 2481–2485. [https://doi.org/10.1007/s10853-005-1979-7]
17. Cullen P.J., Milosavljević V. Spectroscopic characterization of a radio-frequency argon plasma jet discharge in ambient air. Progress of Theoretical and Experimental Physics, 2015, 2015(6), 063J01. [https://doi.org/10.1093/ptep/ptv070]
18. Kvasnytskyi, V., Korzhyk, V., Kvasnytskyi, V., Matviienko, M., Buturlia, Y. Designing brazing filler metal for heat-resistant alloys based on ni al intermetallide. Eastern-European Journal of Enterprise Technologies, 2020, 6(12), 6–19. [http://dx.doi.org/10.15587/1729-4061.2020.217819]
19. Ata F., Calık A., Ucar N. Investigation on the microstructure and mechanical properties of ASTM A131 steel manufactured by different welding methods. Advances in Materials Science, 2022, 22, 4(74), 32–40. [https://doi.org/10.2478/adms-2022-0017]
20. Garcia-Allende P.B., Mirapeix J., Cobo A., Conde O.M. Arc welding quality monitoring by means of near infrared imaging spectroscopy. Proceedings of SPIE – The International Society for Optical Engineering, 2008, 6939. [https://doi.org/10.1117/12.770246]
21. Zhang Y.M., Yang Y.P., Zhang W., Na S.-J. Advanced welding manufacturing – An analysis and review of challenges and solutions. Journal of Manufacturing Science and Engineering, 2020, 142(11), 1–77. [https://doi.org/10.1115/1.4047947]
22. Mirapeix J., Cobo A., Jauregui C., López-Higuera J.M. Fast algorithm for spectral processing with application to on-line welding quality assurance. Measurement Science and Technology, 2006, 17(10), 2623. [https://doi.org/10.1088/0957-0233/17/10/013]
23. Lonkwic P., Tofil A. Supporting welding work in the aspect of increasing production process efficiency. Advances in Science and Technology Research Journal, 2023, 17(1), 8–14. [https://doi.org/10.12913/22998624/157418]
24. Bebiano D., Alfaro S.C.A. A weld defects detection system based on a spectrometer. Sensors, 2009, 9(4), 2851–61. [https://doi.org/10.3390/s90402851]
25. Murphy A.B. The effects of metal vapour in arc welding. Journal of Physics D: Applied Physics, 2010, 43(43), 434001. [https://doi.org/10.1088/0022-3727/43/43/434001]
26. Weglowski M. Investigation on the electric arc light emission in TIG welding. International Journal of Computational Materials Science and Surface Engineering, 2007, 1(6). [https://doi.org/10.1504/IJCMSSE.2007.017927]
27. Uhrlandt D., Kozakov R., Gött G., Wendt M., Schopp H. Temperature profiles of welding arcs and its interpretation. IEEE International Conference on Plasma Science, 2012. [https://doi.org/10.1109/PLASMA.2012.6383562]
28. Nagi Ł., Kozioł M., Zygarlicki J. Comparative analysis of optical radiation emitted by electric arc generated at AC and DC voltage. Energies, 2020, 13(19), 5137. [https://doi.org/10.3390/en13195137]
29. Zhang Y., Wang Q., Liu Y. Adaptive intelligent welding manufacturing. Welding Journal, 2021, 100(1), 63–83. [https://doi.org/10.29391/2021.100.006]
30. Utsumi A., Matsuda J., Yoneda M., Katsumura M. Effect of base metal travelling direction on TIG arc behaviour. Study of high-speed surface treatment by combined use of laser and arc welding (Report 4). Welding International, 2002, 16(7), 530–536. [https://doi.org/10.1080/09507110209549571]
31. Gauglitz G., Moore D.S. Handbook of spectroscopy: second, enlarged edition. – Wiley-VCH Verlag GmbH & Co. KGaA, 2014, 1878. [https://doi.org/10.1002/9783527654703]
32. NIST Standard Reference Database 78. Version 5.11. December 2023, Version History & Citation Information. [https://dx.doi.org/10.18434/T4W30F]
33. Plasma Diagnostic Techniques. Edited by R. H. Huddlestone and S.L. Leonard. Academic Press, 1965, 627. Published online by Cambridge University Press: 13 March 2009. [https://dx.doi.org/10.1017/S0022377800003160]
34. Xiong Q., Nikiforov A., Britun N., Snyders R., Leys

C., Lu X. A simple profile-fitting method to determine the metastable and resonant densities in a cold atmospheric pressure argon plasma jet. Journal of Applied Physics, 2011, 110(7), 073302–073302-10. [https://dx.doi.org/10.1063/1.3643004]

35. Unsöld A., Baschek B. Spektren und Atmosphären der Sterne. In: Der neue Kosmos. Springer Spektrum, Berlin, Heidelberg, 2002, 200-279. [https://doi.org/10.1007/978-3-662-06529-7_7]
36. Nikiforov A. Yu., Leys C., Gonzalez M.A., Walsh J.L. Electron density measurement in atmospheric pressure plasma jets: Stark broadening of hydrogenated and non-hydrogenated lines. Plasma Sources Sci. Technol., 2015, 24, 034001. [https://dx.doi.org/10.1088/0963-0252/24/3/034001]
37. Gigosos M., González-Herrero D. Stark broadening calculations for plasma diagnostics. Conference: Frontiers in Low Temperature Plasma DiagnostisAt: Kerkrade (Netherlands) Ordinal: 10th, 2013. [https://dx.doi.org/10.13140/RG.2.2.29380.22406]
38. Park S., Choe W., Moon S.Y., Yoo S.J. Electron characterization in weakly ionized collisional plasmas: from principles to techniques. Advances in Physics: X, 2019, 4(1), 1526114. [https://doi.org/10.1080/23746149.2018.1526114]
39. Schuller F., Behmenburg W. Perturbation of spectral lines by atomic interactions. Physics Reports, 1974, 12(4), 273–334. [https://doi.org/10.1016/0370-1573(74)90018-0]
40. Foley H.M. The pressure broadening of spectral lines. Phys. Rev., 1946, 69, 616. [https://doi.org/10.1103/PhysRev.69.616]
41. Korzhyk V.M., Grynyuk A.A., Khaskin V.Yu., Voitenko O.M., Burlachenko O.M., Khuan O.O. Plasma-arc technologies of additive surfacing (3D printing) of spatial metal products: application experience and new opportunities. The Paton Welding Journal, 2023, 11, 3–20. [https://doi.org/10.37434/tpwj2023.11.01]
42. Muñoz J., Dimitrijević M.S., Yubero C., Calzada M.D. Using the van der Waals broadening of spectral atomic lines to measure the gas temperature of an argon–helium microwave plasma at atmospheric pressure. Spectrochimica Acta Part B: Atomic Spectroscopy, 2009, 64(2), 167–172. [https://doi.org/10.1016/j.sab.2008.11.006]
43. Fialko N.M., Stepanova, A.I., Navrodska R.O., Gnedash G.O., Shevchuk S.I. Complex methods for analysis of efficiency and optimization of heat-recovery systems. Science and Innivation, 2021, 17(4), 11–18. [https://doi.org/10.15407/scine17.04.011]
44. Ochkin V.N. Spectroscopy of low temperature plasma. – Wiley-VCH Verlag GmbH & Co. KGaA, 2009. – 609. [https://doi.org/10.1002/9783527627509]
45. Lim J.S., Hong Y.J., Ghimire B., Choi J., Mumtaz S., Choi E.H. Measurement of electron density in transient spark discharge by simple interferometry. Results in Physics, 2021, 20, 103693. [https://doi.org/10.1016/j.rinp.2020.103693]
46. Ling S.H. A new neural network structure: node-to-node-link neural network. Journal of Intelligent Learning Systems and Applications, 2010, 2(1). [https://doi.org/10.4236/jilsa.2010.21001]